

CHAPTER 2:
LITERATURE REVIEW

CHAPTER 2

LITERATURE REVIEW

2.1 Introduction

Lithium ion batteries are the prominent choice of power sources in the consumer electronic market today because of the high the energy density that can be delivered. Although a lot of lithium ion batteries are in the market, they are still the object of intense R&D aimed at further improvements of performance through the search of new anode materials as alternatives to the standard carbonaceous compounds without compensating safety requirements.

2.2 Anode materials for lithium ion rechargeable batteries

Megahed and Ebner (1995) have listed some criteria for the selection of anode materials that can be applied in rechargeable lithium ion batteries. These are:

1. High reversible discharge capacity which is more than 372 mAh g^{-1}
2. Low surface area for improved safety i.e. less than $10 \text{ m}^2 \text{ g}^{-1}$
3. High true density i.e. more than 2.0 g cm^{-3}
4. Compatibility with electrolyte solutions and binders
5. Dimensionally and mechanically stable
6. Available at reasonably price

Chen *et al.*, (2001) on the other hand have been pointed out other requirements of a lithium insertion electrode which are good electronic conductivity and good lithium ion conductivity. The structural stability of a host electrode to the repeated insertion and

extraction of lithium ion is undoubtedly one of the key properties for ensuring that a lithium ion cell operates with good electrochemical efficiency.

In transition metal oxides, both stability of the oxygen ion array and minimum displacement of the transition metal cations in the host are both required to ensure good reversibility. Structures with a cubic close packed (ccp) oxygen array are more stable to lithium insertion-extraction than hexagonal close packed (hcp) structures [Thackeray, 1997]. Tabulated in Table 2.1 is the list of component materials for lithium ion batteries. Table 2.2 listed the specific and volumetric capacities for lithium ion battery anode materials.

Table 2.1: Lists of components for lithium ion batteries.

| Anode | Electrolytes | Cathode | Voltage (V) | Current ($\mu\text{A cm}^{-2}$) | Capacity | References |
|--------------------------|---|---------------------------|-------------|-----------------------------------|--------------------------------------|----------------------------------|
| Li | $\text{Li}_{3.6}\text{Si}_{0.6}\text{P}_{0.4}\text{O}_4$ | TiS_2 | 2.5 | 16 | $45\text{-}150 \mu\text{Ah cm}^{-2}$ | Kanehori <i>et al.</i> , (1983) |
| LiV_2O_5 | LiPON | V_2O_5 | 3.5-3.6 | 10 | $6 \mu\text{Ah cm}^{-2}$ | Baba <i>et al.</i> , (1999) |
| V_2O_5 | LiPON | LiMn_2O_4 | - | >2 | $18 \mu\text{Ah cm}^{-2}$ | Baba <i>et al.</i> , (1999) |
| Li/LiI | $\text{LiI-Li}_2\text{S-P}_2\text{S}_5\text{-P}_2\text{O}_5$ | TiS_2 | 1.8-2.8 | 300 | 70mAh g^{-1} | Jones and Akridge (1992) |
| Cu | LiPON | LiCoO_2 | 4.2-3.5 | 1-5 | $130 \mu\text{Ah cm}^{-2}$ | Neudecker <i>et al.</i> , (2000) |
| SiSnON | LiPON | LiCoO_2 | 2.7-4.2 | ~5000 | $340\text{-}450 \text{mAh g}^{-1}$ | Neudecker <i>et al.</i> , (1999) |
| SnO | $\text{Li}_{1.6}\text{V}_{0.61}\text{Si}_{0.39}\text{O}_{5.36}$ | LiCoO_2 | 1.5-2.7 | 1-200 | $4\text{-}10 \mu\text{Ah cm}^{-2}$ | Jones and Akridge (1992) |

2.2.1 Lithium metal

The recent commercial lithium ion batteries used lithium metal as anode. Lithium ion is the most electronegative ion exhibits -3.04 V versus standard hydrogen electrode and lithium is the lightest element in the periodic table (6.94 g mol^{-1}). The specific gravity of lithium metal is 0.53 g cm^{-3} and its specific capacity as anode is 3.86 Ah g^{-1} .

Nevertheless batteries employing lithium metal anodes are prone to safety problems. Cycling the lithium metal anode battery leads to dendrite growth on the lithium anode that can reduce the cycle life.

Table 2.2: Characteristics of some anode materials for lithium battery.

| Materials | Specific capacity (Ah g ⁻¹) | Volumetric capacity (Ah cm ⁻³) | References |
|---|--|---|--|
| Li | 3.861 | 2.060 | Patil <i>et al.</i> , (2008) |
| Li ₂ Sn ₅ | 0.790 | 2.023 | Patil <i>et al.</i> , (2008) |
| Li ₂ Si ₅ | 2.012 | 2.374 | Patil <i>et al.</i> , (2008) |
| Li ₃ Sb | 0.564 | 1.788 | Patil <i>et al.</i> , (2008) |
| Li ₃ As | 0.840 | 2.041 | Patil <i>et al.</i> , (2008) |
| LiAl | 0.790 | 1.383 | Patil <i>et al.</i> , (2008); D'Andrea <i>et al.</i> , (2000) |
| LiC ₆ | 0.339 | 0.760 | Patil <i>et al.</i> , (2008); Cao <i>et al.</i> , (2001); Nishijima <i>et al.</i> , (1997) |
| C (Graphite) | 0.372 | - | Huang <i>et al.</i> , (2007) |
| Li ₂ Ti ₃ O ₇ | 0.298 | - | Van Thournout <i>et al.</i> , (2007); Shu (2008) |
| Li ₄ Ti ₅ O ₁₂ | 0.292 | - | Shu (2009) |
| NiSi ₂ | 0.600 | - | Wen <i>et al.</i> , (2006) |
| Li ₂₂ Sn ₄ | 0.782 | - | Cao <i>et al.</i> , (2001) |
| Si | 4.000 | - | Bourderau <i>et al.</i> , (1999) |
| LiB | 0.452 | - | Zhou <i>et al.</i> , (2006) |
| Sn | 0.800 | - | Chen <i>et al.</i> , (2007) |
| Li _{4,4} Si | 1.967 | - | Si <i>et al.</i> , (2009) |
| Vanadium nitride | 1.236 | - | Sun and Fu, (2008) |
| Si/SnSb | 1.017 | - | Guo <i>et al.</i> , (2006) |
| Sn ₂ BPO ₆ | 0.500 | - | Wan <i>et al.</i> , (1998) |

Dendrite can grow long enough to protrude the separator and come into contact with the cathode to produce an electric short circuit. These causes the batteries self-heat and sometimes ignite. The freshly formed elemental lithium (dendrite) and the organic electrolyte at the anode and electrolyte interface during cell recharging can form films on the anode surface and leads to a corresponding loss of lithium metal [Basu, 1999]. The electric short circuit also can cause a spark that can lead to localized melting and

spreading resulting in a risk of generating a pool of molten lithium due to overheating [Basu, 1999].

2.2.2 Carbonaceous materials

Carbonaceous materials are now used as anode materials in secondary lithium-ion. These materials can intercalate lithium ions, cheap, nontoxic and have no dendrite problem during the charge and discharge processes.

2.2.2.1 Graphite

The most commercial anode materials available in markets are based on graphite elements. Graphite is an allotrope of carbon. Its structure consists of graphene layers stacked in a staggered array usually denoted as ABABABAB along the c-axis. The layers are held together by weak van der Waals forces and the structure is depicted in Figure 2.1. Theoretical capacity of graphite is 372 mAh g^{-1} [Deschamps and Yazami, 1997; Menachem *et al.*, 1998].

Natural graphite powder, modified graphite powder, mesocarbon microbeads (MCMB) and mesocarbon fiber (MCF) are forms of graphite [Takamura, 2002]. Natural graphite does not accept lithium ions easily due to its restricted open area of the edge plane compared to MCMB and MCF which have a larger edge surface convenient for filling the charge carrier under high current charge-discharge. Figure 2.2 shows the micrograph of the outer surface of MCF coated by a thin hard skin as protection to minimize volume expansion and so as to prolong the cycle life.

Graphite is favoured primarily due to its have high lithium intercalation capacity up to 372 mAh g^{-1} and its have low, flat lithium intercalation voltage curve. The low and flat

lithium intercalation potential of graphite which is 100 mV versus Li is a desirable factor for the maintenance of a flat cell voltage output, and to maximize energy density of the cell. The limitation of graphite is low discharge rate capability limiting it in a wide field of applications [Huang *et al.*, 2001].

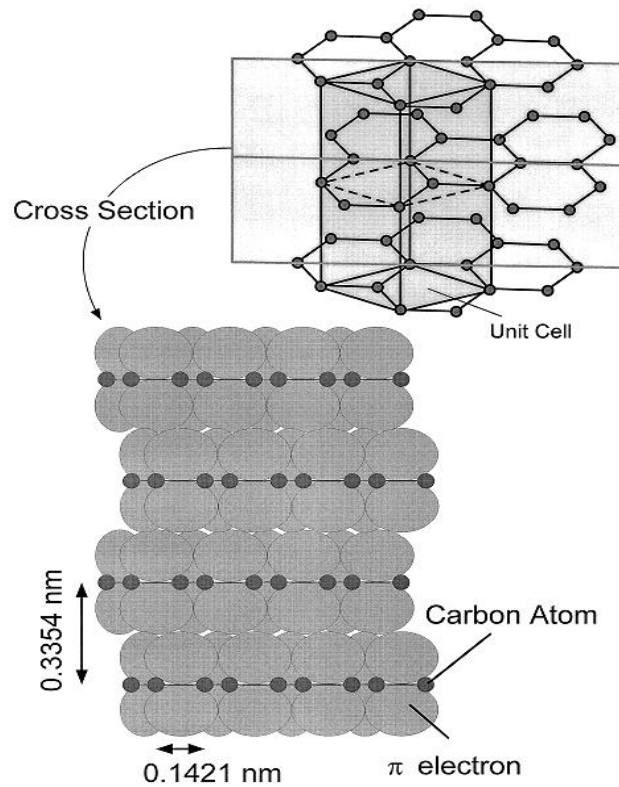


Figure 2.1: Structure of hexagonal graphite showing ABAB stacking and schematic of cross-section of stacking layers considering the thickness of each carbon layer [Azuma *et al.*, 1999].



Figure 2.2: Micrograph of a mesocarbon fiber (MCF) [Takamura, 2002].

2.2.2.2 Soft carbon

Soft carbon is called a graphitizing carbon because it can be graphitized by heat treatment over 2000 °C [Azuma *et al.*, 1999]. Petroleum coke and carbon black [Kinoshita and Zaghbi, 2002] are examples of soft carbon. Shown in Figure 2.3 is the structure of soft carbon based on Franklin model on the randomly oriented layers.

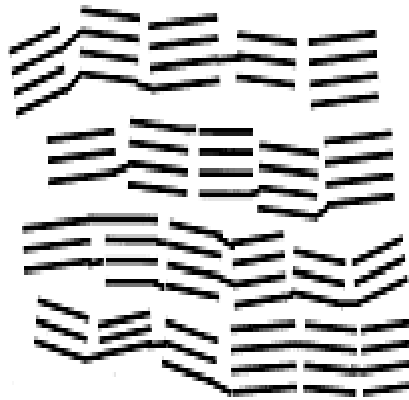


Figure 2.3: Structure of soft carbon [Azuma *et al.*, 1999].

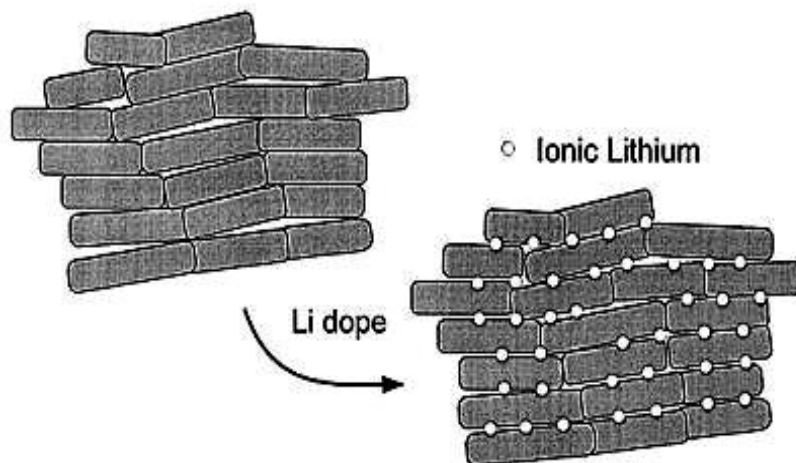


Figure 2.4 Structure of soft carbon before and after doped with lithium ions [Azuma *et al.*, 1999].

Azuma *et al.*, (1999) pointed out that soft carbon is non-porous. Lithium in soft carbon must be in an almost fully ionic state because the electron density in soft carbon is lower than in graphite. The structure of lithium doped soft carbon is illustrated in Figure 2.4.

Coke is an impure form of carbon. It can be obtained by destructive distillation of coal or petroleum. Coke is an amorphous material. Depending on the specific coke material, the reversible capacity is in the range between 160 and 220 mAh g⁻¹ [Shi, 1998]. According to Shi (1998) the size of the carbon layer in the coke is much smaller than that of the graphite where the average size of the carbon layers is 10-20 Å for a coke and 500-1000 Å for graphite. Consequently, smaller size of coke carbon layers can significantly accelerate the solid ionic diffusion process and therefore results in a faster lithium insertion reaction compared to anode based graphite materials.

Pitch coke, fluid coke, needle coke and petroleum coke is promising suitable for anode materials. Fluid coke consists of spherulitic grains with a spherical layer structure that is less graphitizable and the particle morphology tends to be granular. Pitch coke have similar morphology with fluid coke but it is more easily graphitizable. In contrast, needle coke has extremely high graphitizability due to the orientation of its structure where crystallite appears to be partially graphitized even at coking temperatures of 1400 °C [Tran *et al.*, 1999].

Petroleum coke exhibits the lowest irreversible capacity loss of 21 %. The irreversible capacity losses of pitch and needle cokes are 24 % and 26 % respectively as listed in Table 2.3.

Table 2.3: Physical properties of various coke materials [Tran *et al.*, 1999; Chen *et al.*, 1995].

| Types of coke | d_{002} (Å) | Density (g cm ⁻³) | Surface area (m ² g ⁻¹) | Fraction of irreversible capacity loss |
|------------------------|------------------|----------------------------------|---|--|
| Pitch coke | 3.41 | 2.09 | 2.3 | 0.24 |
| Fluid coke | 3.47 | - | 6.8 | - |
| Needle coke | 3.45 | 2.13 | 2.6 | 0.26 |
| Petroleum coke C342 | 3.47 | 2.15 | 6.4 | 0.21 |

Qiu and co-workers (1996) had found that a cell consists of the coke as anode, 1 M LiClO₄-PC-EC-DME as non-aqueous electrolyte and lithium foil as reference electrode is free from the dendrite problem after fifteen cycles. There are no changes in the surface morphology and therefore no issues on short-circuiting. Ma *et al.*, (1996) obtained the highest charge and discharge capacity for needle coke being 236.3 mAh g⁻¹ and 235.5 mAh g⁻¹ respectively compared to other types of coke

2.2.2.3 Hard carbon

Hard carbon is amorphous. It exhibits high capacity and is low cost. Glassy carbon and activated carbon are examples of hard carbon [Kinoshita and Zaghbi, 2002]. At low temperature, intercalation lithium ions in hard carbon exist as ions and as pseudo-metal [Azuma *et al.*, 1999]. Figure 2.5 shows the isolated-layer structure of hard carbon before and after doping with lithium ions.

The initial irreversible capacity of hard carbon is quite large, leading to very low coulombic efficiency at the first cycle. Attempts were tried to improve the performance of hard carbon by modification of the precursors of hard carbon. Chemical pre-treatment

with n-butyl lithium has also been performed. Unfortunately, the initial irreversible capacity of hard carbon still remains to be too large for its practical application.

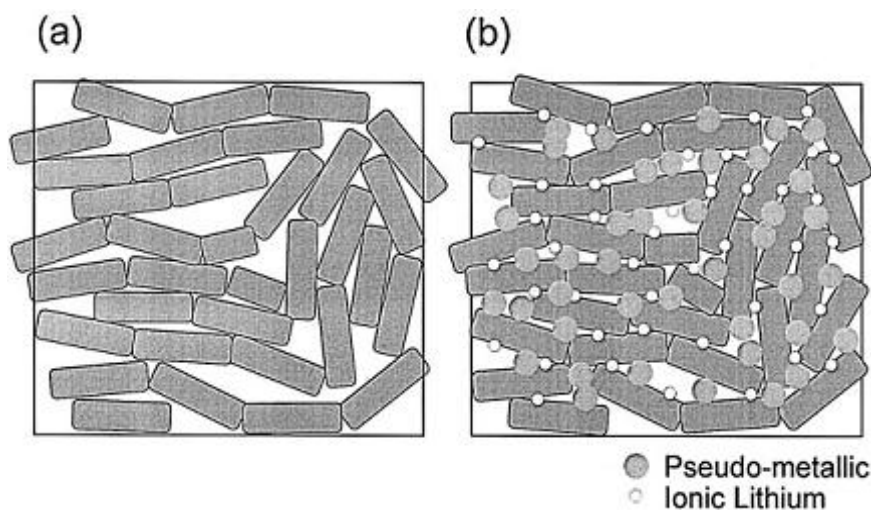


Figure 2.5: Structure of hard carbon before and after doped with lithium ion [Azuma *et al.*, 1999].

The hard carbon/ $\text{Li}_{2.6}\text{Co}_{0.4}\text{N}$ composite anode was prepared for successfully eliminating the initial irreversible capacity of hard carbon [Wissler, 2006]. However the poor cycling performance and critical synthesis condition of $\text{Li}_{2.6}\text{Co}_{0.4}\text{N}$ makes the above mentioned composite anode difficult for practical use. Hard carbons consist of highly unstructured graphene layers. The starting materials are resins or similar products, which are carburized and baked.

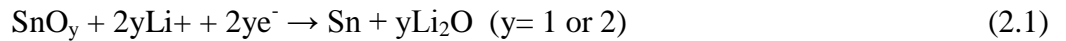
With carbonaceous materials concerned safety issues include the formation of passivation layer at the first charging which consumes lithium from the cathode [Wang *et al.*, 1999]. The possible compounds of this layer are Li_2CO_3 , C-H bonds and $-\text{COOH}$ groups [Matsumura *et al.*, 1995]. This layer tends to decompose at high temperatures and leading to induced cell failure. During long term charge-discharge processes, the passive film could be blocked and slightly formed unstable lithium powder or known as dendrites. Cell using anodes prepared from these materials exhibit huge initial capacity

loss, large volume expansion during charging, poor cycle ability, low working voltage, low power, low conductivity and low reliability for safety.

Jiang and Dahn (2004) found that $\text{Li}_{0.81}\text{C}_6$ is thermally stability with LiPF_6 -based electrolytes compared to pure EC/DEC solvent due to apparent of LiF in the surface of film. Basu (1999) reported negligible cell voltage loss ($\sim 30 \text{ mV}$ - 35 mV) and high anode thermally stability up to the $375 \text{ }^\circ\text{C}$ when a cell consists of $\text{LiC}_6/\text{Li}^+/\text{NbSe}_3$.

2.2.3 $\text{Li}_{4.4}\text{Sn}$

Sn-based materials gained momentum after the report of nearly 600 mAh g^{-1} reversible capacity observed in amorphous Sn-based composite oxides (ATCO) [Idota *et al.*, 1997]. The Sn-oxide is irreversibly reduced to metallic Sn and Li_2O during the first discharge followed by the alloying of Sn with Li, which can be written as:



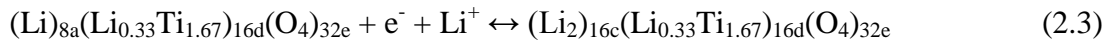
Reaction (2.1) leads to the formation of nano-structured Sn which is homogeneously dispersed in the inactive Li_2O matrix and reaction (2.2) is reversible and responsible for the capacity. However, the $\text{Li}_{4.4}\text{Sn}$ alloy formation involves a large volume change of 300 % for the Sn matrix resulting in cracks and electrode crumbling. These cause loss in electrical contact and capacity fade on repeated cycling [Courtney *et al.*, 1999; Winter *et al.*, 1998].

2.2.4 $\text{Li}_2\text{Ti}_3\text{O}_7$

$\text{Li}_2\text{Ti}_3\text{O}_7$ can be considered as anode materials in advanced lithium-ion batteries [Kataoka *et al.*, 2008]. Chen *et al.*, (2005) and Dompablo *et al.*, (2000) reported that $\text{Li}_2\text{Ti}_3\text{O}_7$ have characteristics of the *Pbnm* space group. Unit cell dimension is $a = 5.012$ Å, $b = 9.540$ Å and $c = 2.942$ Å. $\text{Li}_2\text{Ti}_3\text{O}_7$ with the ramsdellite-type structure is well known to be a fast Li-ion conductor with a conductivity of 4.6×10^{-4} S cm^{-1} at 300 °C [Boyce and Mikkelsen, 1979]. Bohnke *et al.*, (2002) reported $\text{Li}_2\text{Ti}_3\text{O}_7$ to have a conductivity of 3×10^{-9} S cm^{-1} at ambient temperature. Reversible lithium intercalation in $\text{Li}_2\text{Ti}_3\text{O}_7$ has been found located at around 1.4 V versus lithium. Structural studies revealed that $\text{Li}_2\text{Ti}_3\text{O}_7$ does not undergo large charges in structure less than 2 % even at high lithium intercalation. This accounts for its good cyclability as an anode material for rocking chair batteries [Aldon *et al.*, 2006]. On the assumption that all Ti^{4+} ions can be reduced to Ti^{3+} , Shu (2009) pointed out that the theoretical capacity of $\text{Li}_2\text{Ti}_3\text{O}_7$ is 298 mAh g^{-1} . Depending the availability of vacancies in the channels much that it is possible to insert 2.28 lithium, the theoretical capacity will be to 198 mAh g^{-1} [Van Thournout *et al.*, 2007].

2.2.5 $\text{Li}_4\text{Ti}_5\text{O}_{12}$

$\text{Li}_4\text{Ti}_5\text{O}_{12}$ spinel has a potential to be used for anode materials in solid-state lithium batteries due to its very flat charge and discharge curves at 1.5 V versus lithium [Gao *et al.*, 2006]. This voltage is above the potential range where most electrolytes or solvents are reduced. Thus solid electrolyte interface (SEI) films do not form at interface [Yang and Gao, 2009]. The origin of the 1.5 V plateau is due to the coexistence of two phases of lithium titanate $\text{Li}_{1.33}\text{Ti}_{1.67}\text{O}_4$ and $\text{Li}_{2.33}\text{Ti}_{1.67}\text{O}_4$ with the following equilibrium of an electrochemical reaction



Here the subscripts stand for the number of equivalent sites with Wyckoff symbols for the space group $Fd3m$. $\text{Li}_{2.33}\text{Ti}_{1.67}\text{O}_4$ is a good electronic conductor. This is because the average oxidation state of Ti is +3.4 in this lithiated phase implying the existence of 60 % Ti^{3+} and 40 % Ti^{4+} in the lattice. $\text{Li}_{2.33}\text{Ti}_{1.67}\text{O}_4$ is a poor conductor due to the full occupancy of the 16c octahedral site by Li^+ [Yao *et al.*, 2008]. The cubic structure of $\text{Li}_4\text{Ti}_5\text{O}_{12}$ can be described in spinel notation as $\text{Li}_{8a}[\text{Ti}_{5/3}\text{Li}_{1/3}]_{16d}\text{O}_4$. In this notation or structure 75 % of the lithium ions are located at the tetrahedral 8a sites. The remaining lithium ions and titanium ions reside at the 16d octahedral positions of space group $Fd3m$ [Chen *et al.*, 2001].

$\text{Li}_4\text{Ti}_5\text{O}_{12}$ is a zero strain material. It exhibits negligible increase in unit cell volume during charge-discharge processes [Jansen *et al.*, 1999; Kanamura *et al.*, 2006; Kavan *et al.*, 2003]. In the cell couple, the positive and negative electrodes are based on transition metal oxide electrodes which have the capability of accommodating a significant amount of lithium within the host electrode. By restricting shallow limits of charge and discharge, the structural integrity of the electrodes is maintained and this permit high cycle-life to be obtained as shown in Figure 2.6.

This material has a theoretical specific capacity of 175 mAh g^{-1} and exhibited a practical specific capacity at maximum 160 mAh g^{-1} after 100 deep discharge cycles. This material was used successfully as anode coupled with promising cathode material such as LiMn_2O_4 or LiCoO_2 to provide a cell with an operating voltage of about 2.5 V.

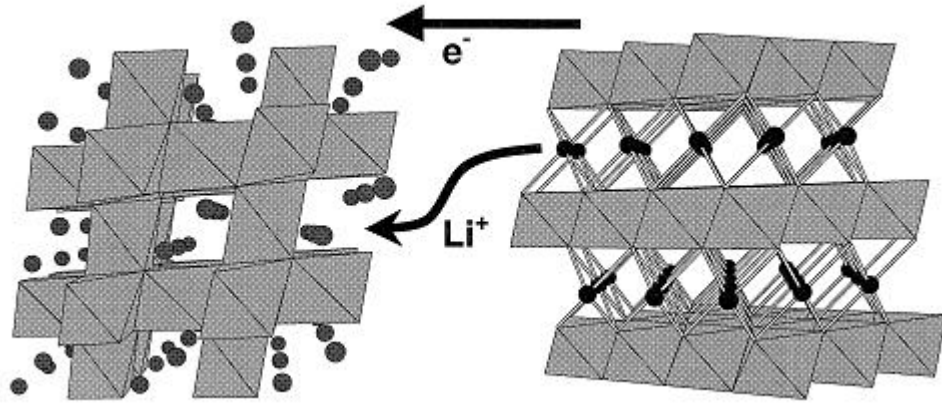


Figure 2.6: Intercalation into the $\text{Li}_4\text{Ti}_5\text{O}_{12}$ spinel and de-intercalation out of the LiCoO_2 layered structure form an ideal cell couple [Jansen *et al.*, 1999].

According to Yao *et al.*, (2005), $\text{Li}_4\text{Ti}_5\text{O}_{12}$ may somewhat eliminate the need of high voltage power sources and the constraint of choosing low voltage anodes. However, according to Gao *et al.*, (2006) the present $\text{Li}_4\text{Ti}_5\text{O}_{12}$ has two major limitations which are:

1. Low conductivity.
2. Bad charge and discharge at heavy current drains.

Wang *et al.*, (2007) and Yao *et al.*, (2008) reported that the electronic conductivity of lithium titanium oxide can be increased by coating this compound with the carbon element such as carbon black. Yang and Gao (2009) have coated $\text{Li}_4\text{Ti}_5\text{O}_{12}$ particles with nano-size (35nm-45 nm) conductive carbon in order to control the particle growth of $\text{Li}_4\text{Ti}_5\text{O}_{12}$ during preparation. According to them, the carbonaceous material partially graphitic material was not incorporated in the $\text{Li}_4\text{Ti}_5\text{O}_{12}$ lattice since the lattice parameter is smaller than uncoated $\text{Li}_4\text{Ti}_5\text{O}_{12}$. Compared with raw $\text{Li}_4\text{Ti}_5\text{O}_{12}$, the $\text{Li}_4\text{Ti}_5\text{O}_{12}$ /composite anode material exhibited higher rate capability and excellent reversibility where the initial discharge capacity of $\text{Li}_4\text{Ti}_5\text{O}_{12}$ /C composite was 174.5

mAh g⁻¹ at 0.5 C and 169.3 mAh g⁻¹ at 1 C, which is very close to the theoretical capacity of Li₄Ti₅O₁₂. The discharge-charge plateau is very flat.

Cu or CuO elements were doped in Li₄Ti₅O₁₂ as the conducting second phase in order to enhance the electronic conductivity [Wang *et al.*, 2009; Huang *et al.*, 2008]. The conductivity of Li₄Ti₅O₁₂ increases as the Cu amount increase from 4.2×10⁻⁷ S cm⁻¹ to 8.2×10⁻⁷ S cm⁻¹ [Wang *et al.*, 2009]. Hao and co-workers (2007) successfully synthesized Li₄Ti₅O₁₂ doped with Cr elements in this system which improved the performance of the electrochemical cell due to stable Cr-O bond in the octahedral coordination polyhedron of the spinel structure. The lattice parameter of Li₄Ti₅O₁₂ tends to be smaller after doping with Al, Ga and Co as listed in Table 2.3 [Huang *et al.*, 2007].

Table 2.4: Lattice parameter for spinel-type Li_{3.95}M_{0.15}Ti_{4.9}O₁₂ (M=Al, Ga and Co) and Li_{3.9}Mg_{0.1}Al_{0.15}Ti_{4.85}O₁₂ materials [Huang *et al.*, 2007].

| Sample | Dopant Element | Ionic dopant radii (nm) | Lattice parameter, <i>a</i> (Å) |
|---|----------------|-------------------------|---------------------------------|
| Li _{3.92} Ti ₅ O _{11.96} | - | - | 8.3716 |
| Li _{3.61} Al _{0.13} Ti _{4.9} O _{11.8} | Al | 0.051 | 8.3693 |
| Li _{3.82} Ga _{0.15} Ti _{4.9} O _{11.94} | Ga | 0.062 | 8.3697 |
| Li _{3.85} Co _{0.15} Ti _{4.9} O _{11.95} | Co | 0.063 | 8.3696 |
| Li _{3.82} Mg _{0.08} Al _{0.14} Ti _{4.85} O _{11.9} | Al, Mg | 0.066 | 8.3682 |

2.3 Previous Li₄Ti₅O₁₂ synthesis technique

Synthesis technique plays an important role in improving the physicochemical properties of the electrode materials. Anode materials have been synthesized by a variety of many techniques such as conventional solid state reaction, sol-gel technique,

ball-milling, spray pyrolysis, molten-salt synthesis, marcoemulsion method and hybrid microwave technique. Each of these methods has its own advantages and limitations.

2.3.1 Solid state reaction

Solid state reaction is the simplest method to synthesize lithium oxide compounds. It involves mechanical mixing of oxides, carbonates and other types of salt and calcination at high temperatures [Shen *et al.*, 2002]. Kataoka and co-workers (2008) prepared $\text{Li}_4\text{Ti}_5\text{O}_{12}$ compound by using this technique. The desired materials such as Li_2CO_3 (99.9%) and TiO_2 (99.9%) were mixed together before it was heated in alumina crucible at 973 K for 12 hours.

Peramunage and Abraham (1998) successfully synthesized the $\text{Li}_4\text{Ti}_5\text{O}_{12}$ by heating the mixture of TiO_2 (anatase) and LiOH at 800 °C followed by grinding and sieving the product to the desired compound. In another method, submicron TiO_2 and Li_2CO_3 were dispersed in hexane and then heated to eliminate the solvent followed by sintering at 800 °C in an oxygen stream to eliminate residues. The morphology studies on $\text{Li}_4\text{Ti}_5\text{O}_{12}$ prepared from LiOH and TiO_2 tend to crystallize and agglomerate to LiOH that melted at a low temperature 450 °C. $\text{Li}_4\text{Ti}_5\text{O}_{12}$ powder synthesized from submicron dimensions fused together to form porous, smaller agglomerates and finer particles because the melting point is 723 °C which is enough for the reaction to proceed without significant growth in the particle size of $\text{Li}_4\text{Ti}_5\text{O}_{12}$. Figure 2.7 shows the SEM micrographs for (a) $\text{Li}_4\text{Ti}_5\text{O}_{12}$ obtained by high temperature solid-state reaction between TiO_2 (anatase) and LiOH and (b) submicron-sized TiO_2 and Li_2CO_3 dispersed in hexane followed by heating.

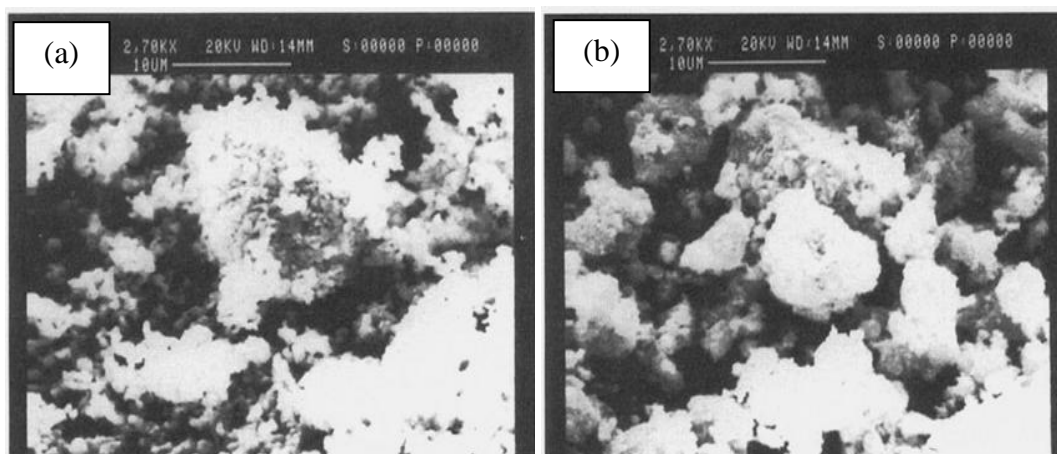


Figure 2.7: SEM images for (a) $\text{Li}_4\text{Ti}_5\text{O}_{12}$ obtained by high temperature solid-state reaction between TiO_2 (anatase) and LiOH and (b) submicron-sized TiO_2 and Li_2CO_3 dispersed in hexane followed by heating [Peramumage and Abraham, 1998].

Unfortunately, the solid-state reaction method requires long-range diffusion of the reactants, has poor control of stoichiometry, exhibits non-homogeneity particles, irregular morphology, large particle size and broad particle size distribution [Yan *et al.*, 2009].

2.3.2 Hybrid microwave technique

The hybrid microwave technique provides a faster route for reactions in the solid state. The method can be carried out at low temperatures and during high reaction and cooling rates, the irradiation of the microwave can form the metastable phases. The starting materials are similar with the solid state technique [Yang *et al.*, 2008].

2.3.3 Ball-milling technique

Anode materials also can be prepared by ball-milling technique. Ball-milling has the capability to reduce particle size, increase surface area and the reactivity of the components [Yan *et al.*, 2009]. Kim *et al.*, (2006) discovered this method using Li_2CO_3 and TiO_2 as the starting materials. These materials were thoroughly mixed in the rotary

mills and pulverized with the ceramic balls for 24 hours. Ethanol was applied as the dispersing medium. The samples were calcinated at 900 °C for five hours followed by ball milling for 24 hours. Then, the powder was sintered at 1050 °C for five hours.

Chen and co-workers (2001) synthesized $\text{Li}_4\text{Ti}_5\text{O}_{12}$ doped with Mg where all the materials were mixed in a mortar and pestle. The mixed powders were ball-milled in methanol followed by drying in an oven at 120 °C. Finally the samples were calcinated at 1000 °C under a 3 % H_2 in He mixture for five hours.

2.3.4 Sol-gel technique

The sol-gel method can be considered as a versatile technique since it can synthesize the starting materials at the molecular level and form high homogeneity multicomponent materials with two or more cations in oxide network [Livage *et al.*, 1997]. The reaction takes places at low temperatures [Kanamura *et al.*, 2006].

Shen *et al.*, (2002) obtained nano-scale particle (100 nm) of $\text{Li}_4\text{Ti}_5\text{O}_{12}$ using the sol-gel method. Citric acid [Gocmez and Fujimori, 2008], oxalic acid [Hao *et al.*, 2006] triethanolamine, TEA [Hao *et al.*, 2005] and acetate acid [Shen *et al.*, 2002] are chelating agents used in the sol-gel method. Isopropyl alcohol was used to decelerate the sol-gel reaction and avoid the emergence of precipitation [Chen *et al.*, 2005]. Bach and co-workers (1999) successfully synthesized $\text{Li}_4\text{Ti}_5\text{O}_{12}$ via the sol-gel process. Titanium isopropoxide, $\text{Ti}(\text{OCHMe}_2)_4$ was added to a solution containing $\text{LiC}_2\text{H}_3\text{O}_2 \cdot 2\text{H}_2\text{O}$ in ethanol. A yellow solution was obtained following the formation of a white gel. The gel was dried for 24 hours. The scanning electron micrographs of the sintered pellets prepared by sol-gel and solid state reaction techniques are displayed in Figure 2.8. As shown in the figure, there is great difference between the two sintered

pellets where the holes in the pellet prepared by sol-gel technique is smaller and much denser than that of the sintered pellet prepared by solid-state reaction.

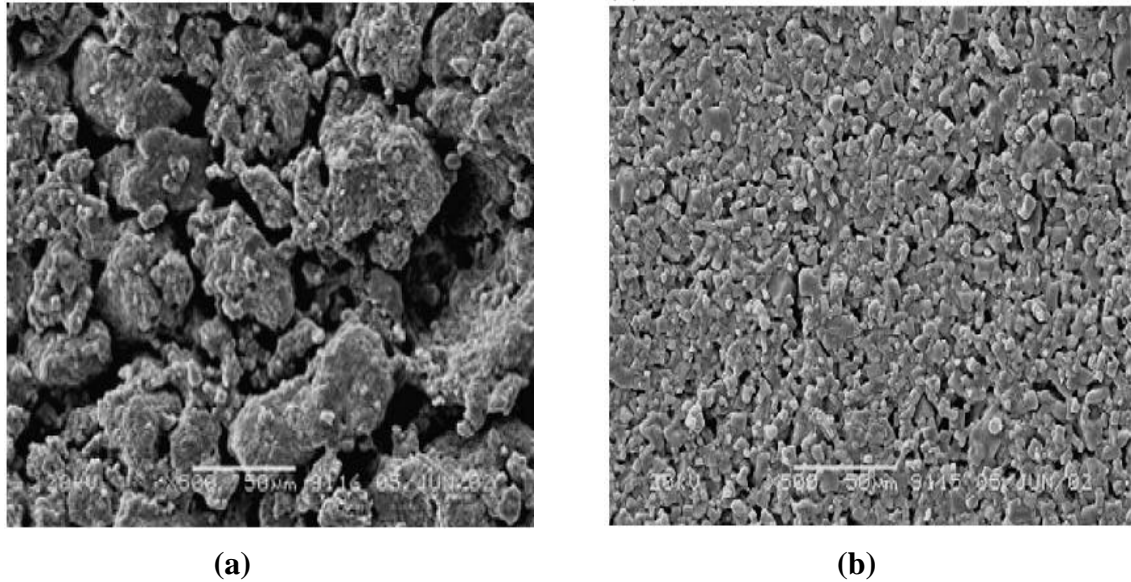


Figure 2.8: SEM micrograph of $\text{Li}_{1.3}\text{Al}_{0.3}\text{Ti}_{1.7}(\text{PO}_4)_3$ sintered pellets prepared by (a) solid-state reaction and (b) sol-gel technique [Wu *et al.*, (2004)].

2.3.5 Blend sample preparation

Particle size is an important factor for improvement of $\text{Li}_4\text{Ti}_5\text{O}_{12}$ performance since smaller size will shorten the diffusion length, increase surface reaction sites, improve lithium intercalation kinetics and hence permitting batteries to operate at higher power [Yuan *et al.*, 2008; Yang *et al.*, 2009]. Yan *et al.*, (2009) synthesized $\text{Li}_4\text{Ti}_5\text{O}_{12}$ via the sol-gel method adopted with ball-milling. The morphology of $\text{Li}_4\text{Ti}_5\text{O}_{12}$ without ball-milling treatment shows a wide particle size distribution and irregular shape. On the other hand, $\text{Li}_4\text{Ti}_5\text{O}_{12}$ with ball-milling treatment have smaller average particle size, narrower particle size distribution and have regular shape. Shown in Figure 2.9 are SEM micrographs of lithium titanate at 800 °C with and without ball-milling treatment.

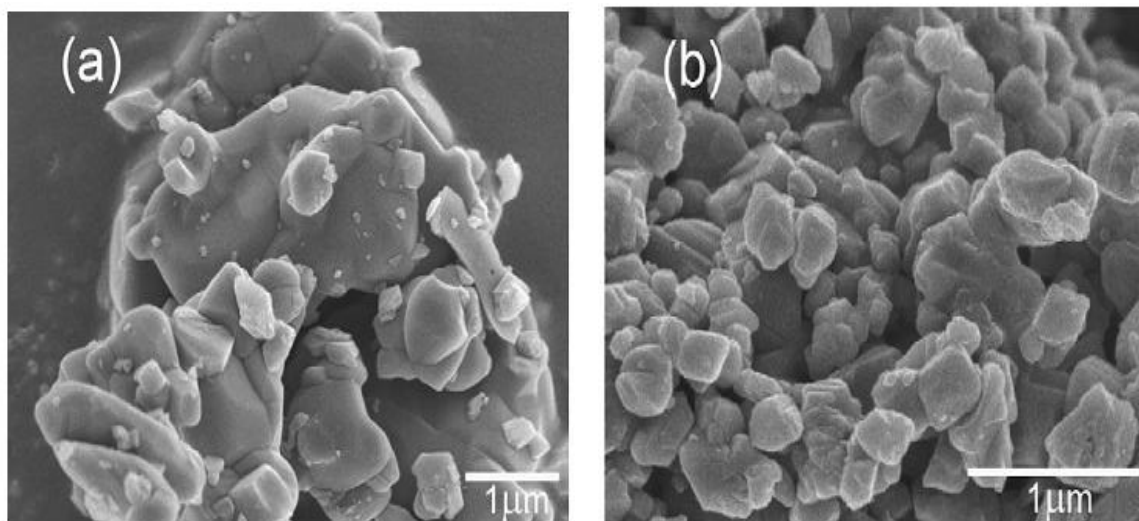


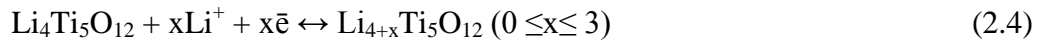
Figure 2.9: SEM images of $\text{Li}_4\text{Ti}_5\text{O}_{12}$ (a) without and (b) with assist ball-milling technique [Yan *et al.*, 2009].

2.4 Electrochemical cell characterization

Electrochemical performance of a cell or battery is strongly dependent on the size, shape and microstructure of the electrode materials.

2.4.1 Charge-discharge

The specific capacity of various samples can be determined using this technique. Kanamura *et al.*, (2006) employed charge-discharge in a potential range of 3.0-1.2 V at 0.1 C rate (16.7 mA g^{-1}) for $\text{Li}_4\text{Ti}_5\text{O}_{12}$ sample. Figure 2.10 shows the charge-discharge curves of $\text{Li}_4\text{Ti}_5\text{O}_{12}$ samples heat-treated at various conditions. All samples exhibited discharge capacity of 160 mAh g^{-1} and it very close to the theoretical capacity which is 167.5 mAh g^{-1} . It can be observed that, a small irreversible capacity was observed in the first cycle, which might be due to an irreversible electrochemical decomposition of the electrolyte. Li^+ ion insertion and extraction takes place in the structure of $\text{Li}_4\text{Ti}_5\text{O}_{12}$ in the course of solid-state redox reaction of $\text{Ti}^{3+/4+}$ as shown in equation (2.4).



The shape of discharge profile of $\text{Li}_4\text{Ti}_5\text{O}_{12}$ depended on the heat treatment condition. It was found that, the flat charge and discharge at 1.55 V versus lithium for samples heat-treated at 800 °C for ten hours (Figure 2.10 (b)) and one hour (Figure 2.10 (c)) is due to intrinsic electrochemical property of $\text{Li}_4\text{Ti}_5\text{O}_{12}$ spinel. Shown in Figure 2.10 (a) is the charge–discharge profile of $\text{Li}_4\text{Ti}_5\text{O}_{12}$ calcined at 500 °C for three hours. Low crystallinity of $\text{Li}_4\text{Ti}_5\text{O}_{12}$ exhibited a small discharge capacity in a potential range from 1.50 V to 1.20 V as detected on the profile. It can be considered that, the discharge capacity in the potential range of 1.50 V-1.20 V is due to Li^+ ion insertion into the glassy phase and the plateau at 1.55 V was attributed to Li^+ ion insertion into the crystalline phase.

2.5 Polymer Composite

Composite materials consisting of ceramic and polymer have been explored due to their high demand in capacitor, acoustic emission sensors and leakage current reduction application. Patsidis and Psarras (2008) have noted that polymer materials are the most convenient materials for development of composite as they are easy to handle during production and processing stages. They have good adhesive properties. They are resistant to corrosive environments and are light weight.

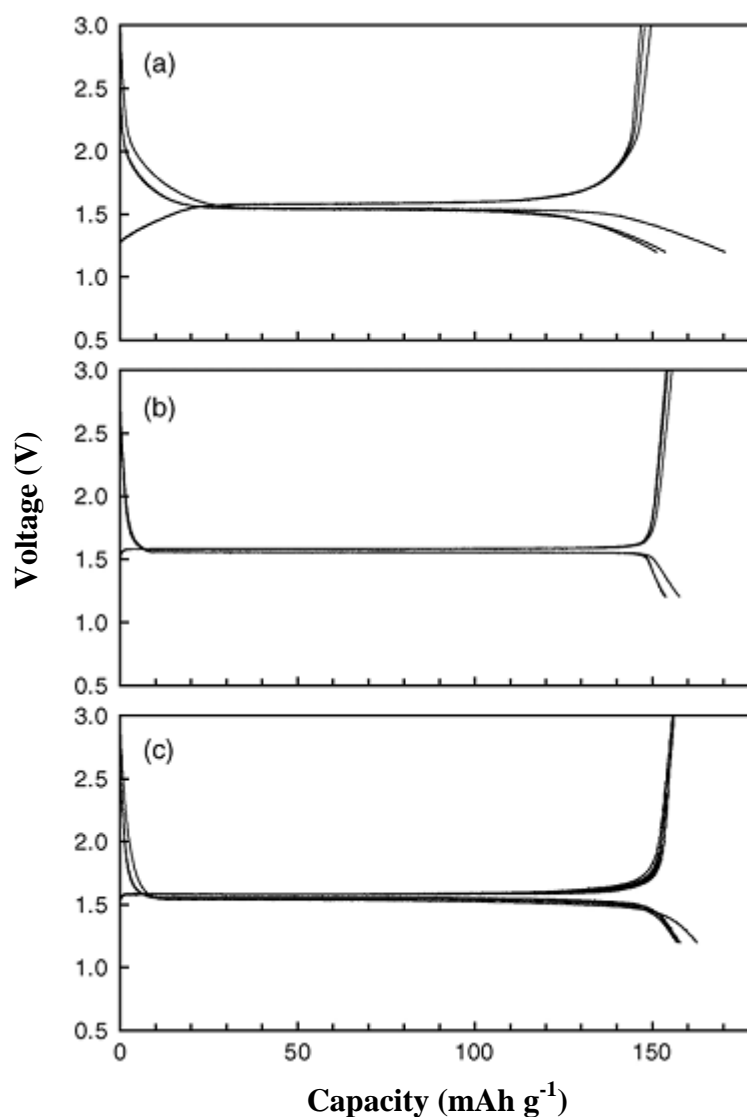


Figure 2.10: Charge and discharge profile of $\text{Li}_4\text{Ti}_5\text{O}_{12}$ samples in 1 M $\text{LiClO}_4/\text{EC} + \text{DEC}$ (1:1 in volume) at 0.1 C rate at various heat treatment (a) 500°C for three hours, (b) 800°C in an electric furnace for ten hours and (c) 800°C in an infrared furnace for one minute [Kanamura *et al.*, 2006].

Unfortunately, polymers are electrical insulators with low dielectric permittivity and often high dielectric strength. On the other hand, ceramic particles are brittle with high dielectric constant and can absorb thermal stress. By combining these materials, the new composite material will exhibit new properties with superior performance.

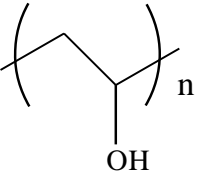
Table 2.5: Previous works on polymer composites.

| Polymers | Ceramic materials | References |
|-----------------------------|---|----------------------------------|
| Epoxy resin | BaTiO ₃ | Patsidis and Psarras (2008) |
| PS | CaCu ₃ Ti ₄ O ₁₂ | Amaral <i>et al.</i> , (2008) |
| Poly (tetrafluoro ethylene) | CaF ₂ | Švorčík <i>et al.</i> , (2005) |
| PVA | ZrO ₂ | Lamastra <i>et al.</i> , (2008) |
| PVA | Al ₂ O ₃ | Lamastra <i>et al.</i> , (2008) |
| PVA | AgNO ₃ | Gautam and Ram (2010) |
| PVdF | BaTiO ₃ | Chanmal and Jog (2008) |
| PVdF | CaCu ₃ Ti ₄ O ₁₂ | Thomas <i>et al.</i> , (2010) |
| PVdF | BaTiO ₃ | Kobayashi <i>et al.</i> , (2008) |
| PVA | BaCl ₂ | Bhajantri <i>et al.</i> , (2006) |

2.5.1 Poly (vinyl alcohol), PVA

Poly (vinyl alcohol), PVA is a synthetic polymer. It has been explored by many researchers and academicians due to unique properties such as ability to form films, biocompatible with high hydrophilic behaviour [Lamastra *et al.*, 2008]. Table 2.6 shows the chemical structure and physical properties of PVA.

Table 2.6: Properties of poly (vinyl alcohol).

| | |
|--|--|
| Chemical Structure |  |
| Boiling point (°C) | 228 °C |
| Melting point (°C) | 230 °C |
| Density (g cm ⁻³) | 1.19-1.31 |
| Amorphous density at 25 °C (g cm ⁻³) | 1.26 |
| Crystalline density at 25 °C (g cm ⁻³) | 1.35 |
| Glass transition temperature (°C) | 85 |

PVA is a semicrystalline polymer [Mohan *et al.*, 2010; Tawansi *et al.*, 2005; Tawansi *et al.*, 1998; Takahashi, 1997]. Gautam and Ram (2010) have prepared nanocomposites of PVA doped with AgNO₃. It was found that, on addition of at least 1 wt. % silver content, the crystallinity of PVA reduces.

2.6 Summary

From the literature survey, graphite is widely applied in lithium-ion battery as anode material. However due to environmental and safety issues, Li₄Ti₅O₁₂ materials is the best candidate to replace the graphite materials due to zero-strain and chemical stability. There are lot of techniques to prepare Li₄Ti₅O₁₂ such as solid-state reaction, hybrid microwave technique and ball-milling method. However sol-gel method is the most versatile technique to obtain small size and homogenous particles. On the hand, PVA has been studied by many researchers as composite materials due to its unique properties. PVA has been doped with different inorganic compounds such BaTiO₃ and CaCu₃Ti₄O₁₂.